MOLECULAR AND CELLULAR BIOLOGY, June 2005, p. 4683–4692 Vol. 25, No. 11
0270-7306/05/$08.00+0 doi:10.1128/MCB.25.11.4683–4692.2005

Smad1 and Smad8 Function Similarly in Mammalian Central Nervous System Development

Mark Hester,[1] John C. Thompson,[1] Joseph Mills,[1] Ye Liu,[1] Heithem M. El-Hodiri,[2] and Michael Weinstein[1]*

Department of Molecular Genetics and Division of Human Cancer Genetics, Ohio State University, 484 W. 12th Ave., Columbus, Ohio 43210,[1] and Center for Molecular and Human Genetics, Columbus Children's Research Institute, and Department of Pediatrics, College of Medicine and Public Health, Ohio State University, Columbus, Ohio 43205[2]

Received 30 September 2004/Returned for modification 2 December 2004/Accepted 3 March 2005

Smads 1, 5, and 8 are the intracellular mediators for the bone morphogenetic proteins (BMPs), which play crucial roles during mammalian development. Previous research has shown that *Smad1* is important in the formation of the allantois, while *Smad5* has been shown to be critical in the process of angiogenesis. To further analyze the BMP-responsive Smads, we disrupted the murine *Smad8* gene utilizing the Cre/*loxP* system. A *Smad8* hypomorphic allele (*Smad8*$^{\Delta exon3}$) was constructed that contains an in-frame deletion of exon 3, removing one-third of the MH2 domain and a small portion of the linker region. *Xenopus* injection assays indicated that this *Smad8* deletion allele is still functional but has reduced ventralizing capability compared to the wild type. Although *Smad8*$^{\Delta exon3/\Delta exon3}$ embryos are phenotypically normal, homozygotes of another hypomorphic allele of *Smad8* (*Smad8*^{3loxP}) containing a neomycin cassette within intron 3, phenocopy an embryonic brain defect observed in roughly 22% of *Smad1*$^{+/-}$ embryos analyzed at embryonic day 11.5. These observations suggest that BMP-responsive Smads have critical functions in the development of the mammalian central nervous system.

Bone morphogenetic proteins (BMPs) are signaling molecules that belong to the transforming growth factor β superfamily, a set of ligands that exert a wide array of biological effects. BMPs were first discovered as the constituent of demineralized bone extracts that could induce the formation of bone and cartilage in rodents (60). Later, BMPs were shown to play important roles in many diverse developmental processes including limb development, axis specification, generation of primordial germ cells, and patterning of the neural tube (37).

To date, there have been eight murine Smad genes identified, with Smads 1, 5, and 8 having been shown to be responsive to BMP signals. Once BMPs are secreted, they bind to type II BMP receptors. These then recruit and phosphorylate type I receptors within intracellular GS (glycine-serine-rich) domains. Type I receptors in turn phosphorylate Smad1, 5, or 8 at the C terminus at a conserved SSXS motif. Smad4, the co-Smad, can then multimerize with the BMP-regulated Smads to facilitate their translocation into the nucleus to either transcriptionally activate or repress target genes (3, 4, 13, 61, 62).

The downstream effects of BMP signaling have been partly elucidated by numerous means, including gene knockout approaches with mice. *Smad1* and *Smad5* have been previously disrupted in other laboratories. *Smad1* null homozygotes die at embryonic day (E10.5) due to defects in the formation of the allantois and placenta (29, 55). *Smad5* null homozygotes also die at E10.5 due to angiogenic failure, mesenchymal apoptosis, and other defects (6, 7, 64).

Although the preceding data have been uncovered through gene knockout approaches with mice, additional BMP functions have been revealed through experimental approaches. For example, a number of laboratories have shown that the establishment of dorsal cell fates within the spinal cord is dependent upon the action of BMP signaling (31). For instance, BMP4 and BMP7 proteins can induce the expression of dorsal cell markers when placed in contact with nonneural ectoderm from chicken explants (11). Conversely, specific ablation of the roof plate in mouse embryos using the conditional expression of diphtheria toxin causes a reduction in dorsal cell markers such as *BMP7*, *Msx1*, and *Zic2* (30). It has been difficult to assess similar roles for specific BMPs in the mouse, probably due to their many redundant functions. However, one example has shown that the deletion of *Gdf7*, a BMP-related molecule expressed in the dorsal neural tube, results in the loss of the D1A interneuron (32).

Though functional analyses of BMP actions in the murine spinal cord have yielded some insights, there is little known about BMP functions in brain development. Interestingly, *BMP2*, *-4*, *-5*, *-6*, and *-7* are coexpressed within the dorsal medial telencephalon, although single knockouts show either an early embryonic lethality, in the case of *BMP2* and *-4*, or show no neural phenotype, as for *BMP5*, *-6*, or *-7* (65). However, double knockouts of *BMP5* and *-7* show defects in neural tube closure, confirming functional redundancies of BMPs within the nervous system (49). *Chrd* and *Nog*, antagonists of BMP signaling (46), have also been shown to be important for proper embryonic brain development in the mouse. *Chrd*$^{-/-}$; *Nog*$^{+/-}$ mice display a number of anterior neuroectodermal abnormalities such as cyclopia, holoprosencephaly, and rostral brain reductions. Embryos doubly homozygous for *Chrd* and *Nog* display forebrain reductions in addition to dorsoventral and left/right patterning defects (1, 5).

* Corresponding author. Mailing address: Department of Molecular Genetics and Division of Human Cancer Genetics, Ohio State University, 484 W. 12th Ave., Columbus, OH 43210. Phone: (614) 688-0164. Fax: (614) 292-4466. E-mail: weinstein.41@osu.edu.

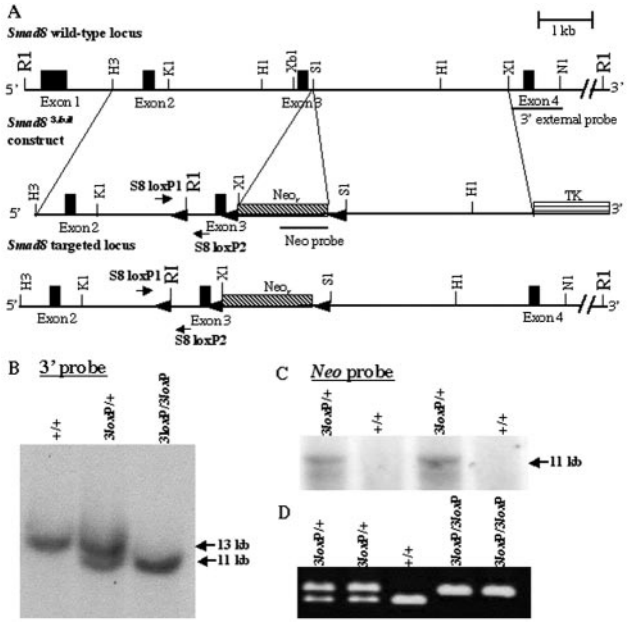

FIG. 1. Targeting the murine *Smad8* gene. (A) Partial map of the *Smad8* genomic locus containing four of the five exons (top), the *Smad8*^{3loxP} targeting vector (middle), and the targeted *Smad8* locus (bottom). (B) Southern blot analysis of tail biopsy DNA confirming correct gene targeting of *Smad8.* Targeting of the *Smad8* locus yields a wild-type 13-kb band and a targeted 11-kb band upon digestion of genomic DNA with EcoRI and hybridization with the 3′ external probe indicated in panel A. (C) Further Southern blot analysis with the same digestion scheme using a neomycin probe confirmed correct targeting. An 11-kb band is detected with a neomycin-specific probe. (D) PCR analysis of tail biopsy DNA extracted from *Smad8*$^{3loxP/3loxP}$ mice. Primers were designed within intron 2 flanking the inserted *loxP* site (A). The lower and upper bands represent the targeted and wild-type alleles, respectively. R1, EcoRI; H3, HindIII; K1, KpnI; H1, HpaI; Xb1, XbaI; S1, SalI; X1, XhoI; N1, NdeI.

To gain further understanding of BMP-responsive Smads in relation to mammalian development, we disrupted the murine *Smad8* gene. Here we report the creation of two hypomorphic alleles for *Smad8*: an in-frame deletion of exon 3 that causes no observable defects and another that contains a neomycin resistance cassette within intron 3. This latter allele causes a partially penetrant reduction in the embryonic midbrain and hindbrain, which is also exhibited by some *Smad1*$^{+/-}$ embryos. Our results show that this phenotype is associated with hypercellularity within the dorsal neuroectoderm, although changes in dorsoventral patterning are not seen.

MATERIALS AND METHODS

Construction of the *Smad8*^{3loxP} targeting vector and generation of *Smad8*$^{\Delta exon3/\Delta exon3}$ mice. A *Smad8* probe containing exons 4 and 5 was used to screen a 129Sv/Ev bacterial artificial chromosome library (43). A 12-kb HindIII fragment of *Smad8* spanning exons 2 through 5 was isolated and subcloned into pBluescript (Stratagene, La Jolla, CA). To generate the *Smad8*^{3loxP} construct (Fig. 1A), a 4.2-kb HindIII/SalI subfragment was isolated, filled in with Klenow, and subcloned into the HpaI site of pLoxPII (63). Another 4.3-kb SalI/XhoI arm of homology was subcloned into the SalI site of pLoxPII, which effectively placed a floxed *PGK-neo* cassette (48) within intron 3. Neomycin was inserted in the forward orientation relative to *Smad8* (Fig. 1A). Lastly, a 43-bp *loxP* site with an engineered flanking EcoRI site was subcloned into an HpaI site within intron 2 of *Smad8*. TC1 129Sv/Ev embryonic stem (ES) cells (8) were electroporated with 50 micrograms of NotI-linearized DNA and selected with ganciclovir and G418 according to the method of Deng et al. (9). DNA from 160 drug-resistant clones was digested with EcoRI and analyzed by Southern blotting using two probes: a 1-kb 3′ external probe and a neomycin probe (Fig. 1B and C, respectively). Of these ES cell clones, two had been successfully targeted to the *Smad8* locus. Correctly targeted clones were injected into C57BL/6 blastocysts, and chimeric mice were generated. Chimeric males were mated with National Institutes of Health (NIH) Black Swiss females, and the offspring were subsequently bred inter se. Once *Smad8*$^{3loxP/3loxP}$ mice were generated, they were bred to *EIIA-Cre* mice (28) to excise the neomycin cassette for the production of *Smad8* floxed and *Smad8*$^{\Delta exon3}$ mice.

Genotype analysis. *Smad8*^{3loxP} mice were genotyped for the presence of the *loxP* site within intron 2 of *Smad8* using PCR (Fig. 1D). Forward and reverse primers were designed flanking the *loxP* site, *S8 loxP*1 (5′-CACAGAAGGAGA GAGGGACGG-3′) and S8 *loxP*2 (5′-TGGATACAGGTTGCCTCACAG-3′). Mice bearing *Smad8*$^{\Delta exon3}$ alleles were genotyped using the *Smad8 loxP*1 primer and S8R (5′-CTATCCTGTCTCACAGCCCTC-3′) located 3′ to the neomycin cassette. *Smad1* genotyping was performed as previously described (29).

Histological analysis and in situ hybridization. E11.5 embryos were dissected free from the uterus and extraembryonic membranes and fixed in 4% paraformaldehyde with rocking at 4°C overnight. The following day, the embryos were dehydrated through an ethanol series, embedded in paraffin, sectioned at 7 μm, and stained with hematoxylin and eosin. Radioactive in situ hybridization was performed using standard procedures. ^{35}S-labeled probes were prepared for *Pax3* (22), *Pax6* (56), *Foxa2* (27), and *Shh* (17).

Neurofilament antibody staining. E11.5 embryos were stained with the 2H3 neurofilament antibody developed by T. M. Jessell and T. Dodd and obtained from the Developmental Studies Hybridoma Bank developed under the auspices of the National Institute of Child Health and Human Development and maintained by the Department of Biological Sciences, University of Iowa, Iowa City, IA.

BrdU cellular proliferation assay. Pregnant mice were subcutaneously injected with 5-bromo-2′-deoxyuridine (BrdU) at 10 μg per gram body weight. After 3 hours, the mice were sacrificed and embryos were prepared as described above. A BrdU in situ detection kit (BD Pharmingen, San Diego, CA) was used to perform immunohistochemical staining against BrdU according to the manufacturer's instructions. Two abnormal *Smad1*$^{+/-}$ embryos and wild-type siblings were evaluated by analysis under high magnification of the number of stained cells within the dorsal neural tube. Three random areas within the dorsal neural tube were analyzed, and mitotic indexes were calculated. Results were shown to be statistically significant with a P value of $<1.0 \times 10^{-4}$.

***Xenopus* injection assay.** The *Smad8* wild-type (WT) or *Smad8* truncated (TD) cDNAs were cloned into the EcoRI site of the pCS2+ vector from a *Smad8* expression vector (42). A *Smad8*$^{\Delta exon3}$ cDNA was generated from an inverse PCR using the *Smad8* expression vector as a template and polyacrylamide gel electrophoreis-purified primers 5′-CAG ACA GTC CCT ATC AAC ACT CAG GTG TG CAT TTG TAC TAC GTT GGG G-3′ and 5′-CCC CAA CGT AGT ACA AAT GCA CAC CTG AGT GTT GAT AGG GAC TGT CTG-3′. The *Smad8*$^{\Delta exon3}$ cDNA was sequenced to verify the absence of mutations and was then cloned into the EcoRI site of the pCS2+ vector. The *Smad8*$^{\Delta exon4,5}$ cDNA vector was constructed by amplifying the first three exons of Smad8 and cloning this fragment into the EcoRI site of the pCS2+ vector. Each of these constructs was linearized with NotI and used as a template to produce mRNA by in vitro transcription using the mMessage mMachine kit (Ambion, Austin, TX). *Xenopus* embryos were prepared and cultured as previously described (18). One nanogram of *Smad8* and derivative mRNAs was injected into the marginal zone of 4-cell-stage embryos. To control for the injection process, β-galactosidase mRNA was injected into the marginal zone of control embryos. A total of 60 *Xenopus* blastulae were injected with the above mRNAs and phenotypically scored utilizing the *Xenopus* dorso-anterior index system (26), and the results were analyzed using an unpaired t test.

Transfections and reporter assays. All culture media and reagents used in this study were acquired from Invitrogen (CA). Bl6 cells were cultured in Dulbecco's modified Eagle's medium with 10% fetal bovine serum supplemented with 60 units/ml penicillin and 60 μg/ml streptomycin. All cell lines were grown in 5% CO_2, 95% humidity at 37°C. For transfections into various cell lines, SuperFect reagent (QIAGEN, Hilden, Germany) was used according to the manufacturer's instructions. Cells were seeded into 12-well dishes at 70 to 80% confluence 24 h before transfection. The amount of DNA per transfection was kept consistent by the addition of an empty expression vector, pCS2+. Cells were harvested 36 h after transfection, rinsed with 1× phosphate-buffered saline, and lysed in 200 μl of reporter lysis buffer (Promega, Madison, WI). Lysates were frozen on dry ice and thawed in a 37°C water bath. For luciferase and β-galactosidase reporter assays, kits were purchased from Promega and used according to the manufac-

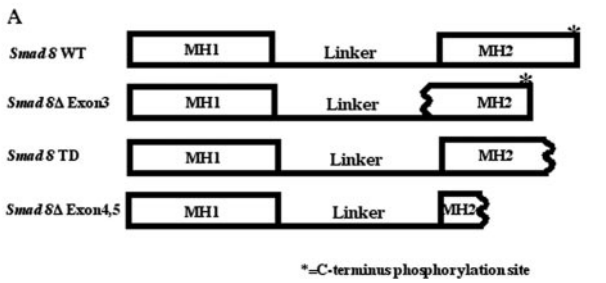

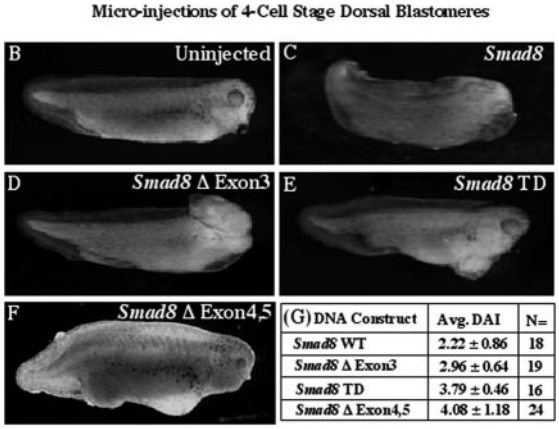

(G) DNA Construct	Avg. DAI	N=
Smad8 WT	2.22 ± 0.86	18
Smad8 Δ Exon3	2.96 ± 0.64	19
Smad8 TD	3.79 ± 0.46	16
Smad8 Δ Exon4,5	4.08 ± 1.18	24

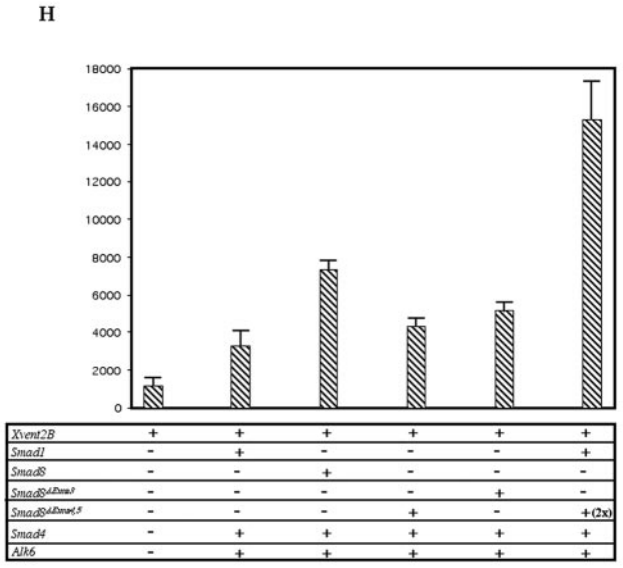

FIG. 2. The *Smad8*$^{\Delta exon3}$ allele acts as a hypomorph in *Xenopus laevis*. (A) Schematic representations of *Smad8* WT, *Smad8*$^{\Delta exon3}$, *Smad8*$^{\Delta exon4,5}$, and *Smad8* TD constructs used for microinjections into four-cell-stage embryos. Wavy lines represent deletion breakpoints. *Smad8*$^{\Delta exon3}$ lacks one-third of the MH2 domain and a small portion of the linker region. *Smad8*$^{\Delta exon4,5}$ lacks the majority of the MH2 domain. *Smad8* TD lacks the C-terminal phosphorylation site. (B) Uninjected embryos develop normally. (C) Microinjection of *Smad8* WT mRNA into dorsal blastomeres ventralizes *Xenopus* tadpoles. (D) Microinjection of *Smad8*$^{\Delta exon3}$ into dorsal blastomeres also ventralizes *Xenopus* tadpoles but to an intermediate extent. (E) *Smad8* TD lacks the majority of the Smad8 ventralizing capability. (F) Microinjection of *Smad8*$^{\Delta exon4,5}$ into dorsal blastomeres also ventralizes *Xenopus* tadpoles but to a lesser extent. Note, β-galactosidase mRNA was coinjected with *Smad8*$^{\Delta exon4,5}$ mRNA in the image shown in panel F. (G) Average (Avg.) DAI scores and numbers of embryos (N) are shown. (H) Results from a luciferase reporter assay utilizing the *Xvent2B* promoter driving luciferase and cDNAs for the following constructs: *Smad1*, *Smad8*, *Smad4*, *Alk-6*, *Smad8*$^{\Delta exon3}$, and *Smad8*$^{\Delta exon4,5}$.

turer's instructions. Experiments were performed in triplicate, and results were normalized to β-galactosidase values. Error bars represent the deviations from the results of at least three independent experiments.

RESULTS

Targeted disruption of the murine *Smad8* gene. A targeting vector was constructed such that exon 3 of the *Smad8* gene was flanked by *loxP* sites (48), while a neomycin resistance cassette (*neo*) was introduced into intron 3 of *Smad8* (Fig. 1A). The *neo* cassette within the targeting vector, driven by the *PGK* promoter, is in the same transcriptional orientation as *Smad8* (Fig. 1A). This allele of *Smad8* will be subsequently referred to as *Smad8*^{3loxP}.

After electroporation and selection with G418 and ganciclovir, ES cell clones were screened by Southern blot analysis (Fig. 1B and C). Correctly targeted clones were injected into C57BL/6 blastocysts to generate chimeric mice. *Smad8*$^{3loxP/+}$ mice were genotyped for the presence of the *loxP* site within intron 2 using PCR (Fig. 1D).

The *Smad8*$^{\Delta exon3}$ allele functions as a hypomorph in *Xenopus* injection assays. To elucidate the functional consequence(s) of deleting exon 3 from *Smad8*, we utilized an in vivo assay with *Xenopus laevis*. Prior research has shown that *Xsmad1*, *Xsmad5*, and *Xsmad8* mRNAs are all capable of ventralizing *Xenopus* tadpoles when injected into the dorsal side of 4-cell-stage embryos, although some homologs of the latter fail to do so (39, 41, 47, 50, 52). Here we show that mouse *Smad8* is similarly capable of ventralizing *Xenopus* embryos. Four *Smad8* mRNAs were injected into *Xenopus* embryos: full-length *Smad8* (*Smad8* WT), *Smad8* lacking exon three (*Smad8*$^{\Delta exon3}$), *Smad8* lacking exons four and five (*Smad8*$^{\Delta exon4,5}$), and a *Smad8* cDNA lacking the C-terminal phosphorylation site (*Smad8* TD) (42) (Fig. 2A). A qualitative analysis utilizing the dorso-anterior index (DAI) indicated that *Smad8* WT mRNA had a ventralizing effect on *Xenopus* embryos compared to uninjected controls (Fig. 2B and C), while *Smad8* TD had an attenuated effect (Fig. 2E). The latter result was expected given the fact that a similar *Smad1* mutant behaves as a dominant negative (45). Although *Smad8*$^{\Delta exon3}$ was able to ventralize *Xenopus* tadpoles, it had a reduced effect compared to wild-type *Smad8* ($P = 5.2 \times 10^{-3}$) (Fig. 2D). This suggests that the *Smad8*$^{\Delta exon3}$ allele could act as a hypomorph rather than as a null mutation of *Smad8* in the mouse. The mRNA made by the *Smad8*^{3loxP} allele, *Smad8*$^{\Delta exon4,5}$, was tested similarly. Interestingly, this allele was also able to weakly ventralize *Xenopus* embryos ($P < 1.0 \times 10^{-4}$) (Fig. 2F). This was quite surprising, as the *Smad8*$^{\Delta exon4,5}$ mutation deletes roughly 75% of the MH2 domain and would be expected to disable the protein. Indeed, a similar allele of *Smad2*, in which the MH2 domain had been deleted, was nonfunctional in *Xenopus* assays (34). DAI scores for the various *Smad8* alleles are shown in Fig. 2G.

Our *Xenopus* assays demonstrated that we had created two

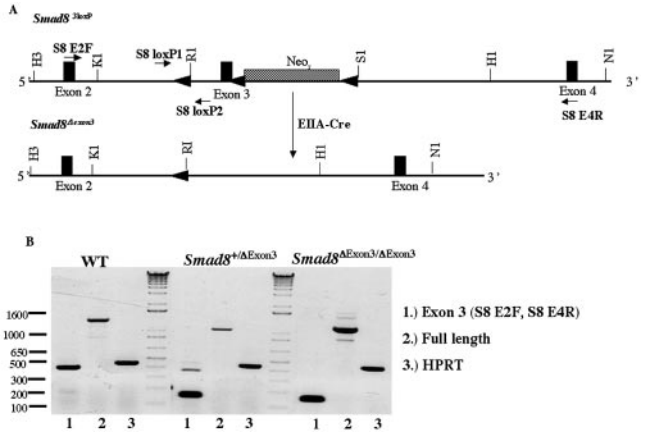

FIG. 3. Cre mediates the excision of exon 3 and *neo* in *Smad8*$^{3loxP/3loxP}$ mice. (A) Schematic diagram of the *Smad8*^{3loxP} allele undergoing the Cre-mediated deletion of *neo* and exon 3 from the *Smad8* locus. (B) RT-PCR analysis illustrating that exon 3 has been excised from *Smad8* in *Smad8*$^{\Delta exon3/\Delta exon3}$ mice. Lanes 1 show PCR products amplified by primers (S8 E2F and S8 E4R) that flank exon 3 and give a product of ~400 bp. The 150-bp band seen in the *Smad8*$^{\Delta exon3/+}$ and *Smad8*$^{\Delta exon3/\Delta exon3}$ samples represent the regions that flank exon 3. Lanes 2 show PCR products of full-length *Smad8.* As a positive control, hypoxanthine phosphoribosyltransferase (HPRT) was used and is shown in lanes 3. Restriction enzyme abbreviations are given in the legend to Fig. 1.

novel hypomorphic alleles of *Smad8*. Although these alleles were not null, we suspected that they might be invaluable, since null *Smad1* and *Smad5* mutants die during early embryogenesis (6, 7, 29, 55, 64). We therefore hypothesized that an analysis of hypomorphic *Smad8* alleles would allow for further dissection of BMP functions throughout mammalian development.

***Smad8*$^{\Delta exon3/\Delta exon3}$ mice are viable and fertile.** *Smad8*$^{3loxP/3loxP}$ mice were mated with *EIIA-Cre* mice, which zygotically express Cre in a mosaic fashion (28). This has previously been shown to efficaciously create excision products from alleles with multiple *loxP* sites (24) and was successful in creating *Smad8*$^{\Delta exon3}$ mice (Fig. 3A). The F_1 generation, resulting from the cross between an *EIIA-Cre* male and a *Smad8*$^{3loxP/3loxP}$ female, produced mosaic offspring, which carried all of the expected excision alleles. F_1 progeny carrying the *Smad8*$^{\Delta exon3}$ allele were mated to wild-type females, and F_2 mice were genotyped again for the *Smad8*$^{\Delta exon3}$ allele and allowed to interbreed. This intercross resulted in *Smad8*$^{\Delta exon3/\Delta exon3}$ mice that were healthy, fertile, and represented at normal Mendelian ratios (data not shown) and that have life spans of approximately 2 years, equivalent to their wild-type siblings. To confirm that exon 3 was absent from the *Smad8* transcript, reverse transcription (RT)-PCR was performed, demonstrating its complete deletion in *Smad8*$^{\Delta exon3/\Delta exon3}$ mice (Fig. 3B). Additionally, the junction between exons 2 and 4 was sequenced and shown to be in frame with the rest of the *Smad8* transcript, as expected (data not shown). The *Smad8*$^{\Delta exon3}$ mutation should result in deletion of amino acids 224 to 298, deleting part of the linker as well as one-third of the MH2 domain of Smad8. Real-time PCR was used to ascertain the level of *Smad8* transcript in *Smad8*$^{\Delta exon3/\Delta exon3}$ mice showing no difference compared to wild-type siblings (data not shown). Therefore, deletion of exon 3 does not appear to affect the stability or steady-state level of the *Smad8* mRNA.

Phenotypic *Smad8*$^{3loxP/3loxP}$ and *Smad1*$^{+/-}$ embryos exhibit partially penetrant midbrain and hindbrain reductions. The presence of an intronic neomycin resistance cassette within a gene can cause aberrant splicing, resulting in a *neo* fusion transcript, due to the presence of strong cryptic splice acceptor and donor sites within the *neo* cassette (38). When neomycin is inserted in the forward orientation relative to gene transcription, the frequency of aberrant splicing is much less than if it is placed in the reverse orientation (40). Indeed, hypomorphic alleles have been created through the intronic placement of *neo* (38).

We therefore tested whether the *neo* cassette could disrupt expression of the *Smad8* gene. Our analysis shows that a *Smad8-neo* fusion mRNA can be detected in the *Smad8*$^{3loxP/3loxP}$ mice (Fig. 4A and B). Sequencing of this *Smad8-neo* fusion product demonstrates that *neo* was spliced in between exons 3 and 4, utilizing a previously described splice site 5 base pairs upstream of the initiating ATG codon (38). This aberrant splicing causes *neo* to be out of frame with the *Smad8* transcript, resulting in a premature stop codon, which ultimately allows for the synthesis of a truncated Smad8 protein lacking roughly three-fourths of the MH2 domain. *Xenopus* assays have suggested that this protein retains partial function (Fig. 2F). To determine the level of wild-type *Smad8* transcript in *Smad8*$^{3loxP/3loxP}$ mice, we employed real-time PCR technology. Our analysis has shown that *Smad8* is reduced in the adult *Smad8*$^{3loxP/3loxP}$ brain (Fig. 4C), confirming that the *Smad8*^{3loxP} allele is hypomorphic (data not shown).

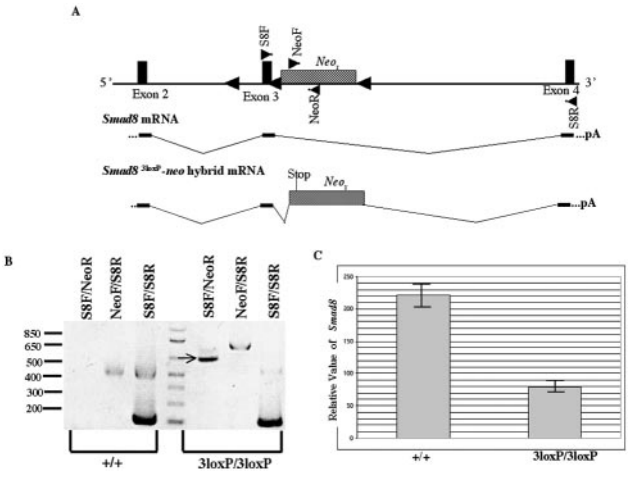

FIG. 4. Aberrant splicing of *neo* within *Smad8* results in a *Smad8-neo* fusion transcript. (A) Schematic diagram of the *Smad8*^{3loxP} allele (top) with primer pairs represented as triangles within exons (S8F and S8R) or in the *neo* cassette (NeoF and NeoR). The *Smad8* transcript is depicted (middle) showing exons 2, 3, and 4. The *Smad8-neo* hybrid transcript found in the *Smad8*$^{3loxP/3loxP}$ mice is spliced in between exons 3 and 4, causing *neo* to be out of frame with the *Smad8* transcript, which results in a premature stop codon within *neo*. (B) RT-PCR analysis of the *Smad8-neo* hybrid transcript, with primer pairs shown on top and the indicated sample cDNA shown below. The PCR product using primer pair S8F-NeoR in the *Smad8*$^{3loxP/3loxP}$ sample indicated by an arrow was sequenced and shown to be a *Smad8-neo* hybrid transcript. (C) Relative level of *Smad8* expression as determined by real-time PCR.

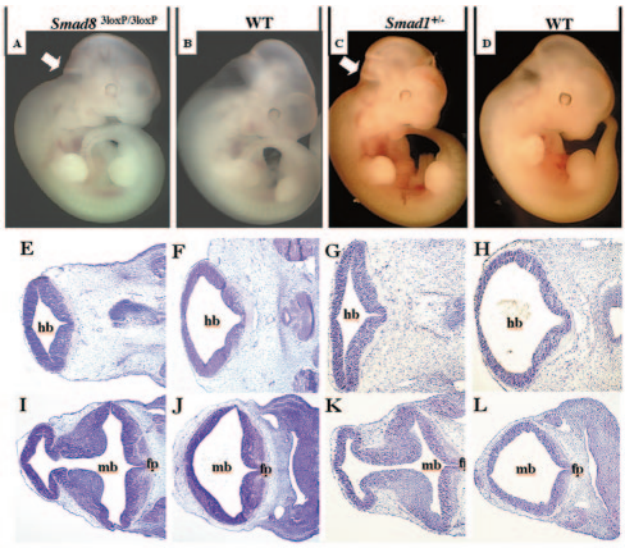

FIG. 5. Phenotypic *Smad8*$^{3loxP/3loxP}$ and *Smad1*$^{+/-}$ embryos display reductions in the hindbrain and midbrain. Genotypes of pictured embryos and sections are shown at the top. (A to D) Whole mount pictures of phenotypic *Smad8*$^{3loxP/3loxP}$(A), littermate control (B), phenotypic *Smad1*$^{+/-}$ (C), and littermate control (D) embryos at E11.5. Note that the hindbrain and midbrain are significantly reduced both in phenotypic *Smad8*$^{3loxP/3loxP}$ and *Smad1*$^{+/-}$ embryos as indicated by arrows. (E to L) Frontal histological sections within the neural tube show reduced space and hypercellularity within the midbrain of phenotypic *Smad8*$^{3loxP/3loxP}$ (I) and phenotypic *Smad1*$^{+/-}$ (K) embryos at E11.5 compared to wild-type siblings (J and L, respectively). More caudal histological sections show the same diminished space within the hindbrain of abnormal *Smad8*$^{3loxP/3loxP}$ (E) and abnormal *Smad1*$^{+/-}$ (G) embryos compared to wild-type siblings (F and H, respectively). mb, hb, and fp inbdicate midbrain, hindbrain, and floor plate, respectively.

To test whether the reduction in *Smad8* levels had an effect on normal development, we observed 45 embryos at E11.5 from *Smad8*$^{3loxP/3loxP}$ intercrosses and found midbrain and hindbrain reductions in 11% of them (Fig. 5A and B). This phenotype was not observed in *Smad8*$^{\Delta exon3/\Delta exon3}$ embryos, suggesting that it is specifically associated with the *Smad8*^{3loxP} allele. There exists the possibility that *neo* might be affecting the expression of neighboring genes, causing this phenotype indirectly. An analysis of the annotated mouse genome through the Ensembl Mouse Genome Browser revealed a single gene in close proximity to *Smad8*, *RFXAP*, an important regulatory gene associated with the major histocompatibility complex class II molecules (15). To address the possibility that the intronic *neo* was affecting genes nearby *Smad8* and causing the observed phenotype, we performed semiquantitative RT-PCR on wild-type and phenotypic *Smad8*$^{3loxP/3loxP}$ embryos and found expression levels for *RFXAP* to be consistent between the two (data not shown).

More intriguingly, we have also identified a partially penetrant lethality in *Smad1* heterozygotes due to previously uncharacterized midbrain/hindbrain defects (Fig. 5C and D). Analyzing intercrosses between *Smad1*$^{+/-}$ and wild-type mice, we have observed a statistically significant reduction ($P < 0.01$) in the number of *Smad1*$^{+/-}$ mice at weaning (Table 1). Although there were no apparent defects in 40 *Smad1*$^{+/-}$ embryos at E9.5 (data not shown), roughly 22% of the E11.5 *Smad1*$^{+/-}$ embryos displayed midbrain and hindbrain reductions (Table 1).

There remains the possibility that the aberrant *Smad8* transcript produced in *Smad8*$^{3loxP/3loxP}$ embryos acts as a dominant inhibitor of Smad1 signaling, thereby recapitulating the nervous system defect observed in *Smad1* heterozygotes. However, the cDNA produced by the *Smad8*^{3loxP} mutants (*Smad8*$^{\Delta exon4,5}$) was injected into *Xenopus laevis* embryos and was shown to possess very weak ventralizing activity (Fig. 2F). This result is indicative of a hypomorphic and not an antimorphic allele. To confirm this, transcriptional reporter assays were carried out utilizing the BMP-responsive *Xvent2B* promoter (23) driving the luciferase reporter gene. The *Xvent2B* promoter exhibited some endogenous activity (Fig. 2H, lane 1) which was increased roughly twofold with the addition of Smad1, Smad4, and a constitutively activated receptor, Alk6 (Fig. 2H, lane 2), in agreement with experiments done previously (23). However, we are now able to demonstrate that Smad8 also transactivates the *Xvent2B* promoter to the same extent as or possibly to a greater extent than Smad1 (Fig. 2H, lane 3.) The *Smad8*$^{\Delta exon4,5}$ cDNA was also capable of transactivating the *Xvent2B* promoter but to a lesser degree than wild-type Smad8 (Fig. 2H, lane 4), as was the *Smad8*$^{\Delta exon3}$ allele (Fig. 2H, lane 5). To test whether the *Smad8*$^{\Delta exon4,5}$ allele could function in an antimorphic fashion and reduce the signaling of the other BMP-regulated Smads, it was expressed alongside wild-type Smad1, to determine whether it could restrict Smad1-mediated activation. However, the *Smad8*$^{\Delta exon4,5}$ protein did not interfere with Smad1-mediated transcription (Fig. 2H, lane 6).

Abnormal *Smad1*$^{+/-}$ embryos exhibit increased cellular proliferation in the dorsal region of the neural tube. Histological analysis reveals that the observed neuroectodermal phenotype in abnormal *Smad1* heterozygous embryos is associated with hypercellularity within the dorsal region of the neural tube (Fig. 5E to L). To address the cause of this hypercellularity, we examined the level of cellular proliferation within the neural tube of abnormal *Smad1*$^{+/-}$ embryos using BrdU (Fig. 6A and D). Higher numbers of labeled cells were found in the dorsal midbrain of *Smad1*$^{+/-}$ embryos than in that of their wild-type siblings (Fig. 6B and E). Interestingly, the number of labeled cells within the ventral neural tube was consistent between *Smad1*$^{+/-}$ and wild-type mice (Fig. 6C and F). Quantitation of the BrdU incorporation showed a 20% increase in the mitotic index on the dorsal side of the neural tube in abnormal *Smad1* heterozygotes compared to the wild type (Fig. 6G). The

TABLE 1. Phenotype and genotype analysis of *Smad1*$^{+/-}$ × WT crosses

Age	No. with phenotype of *Smad1*$^{+/-}$		No. observed with genotype (no. expected)		Total no. of mice
	Normal	Brain reduction	+/+	+/−	
E11.5	32	9	37 (39)	41 (39)	78
Postnatal	NA[a]	NA	102 (80)	58 (80)	160

[a] NA, not applicable.

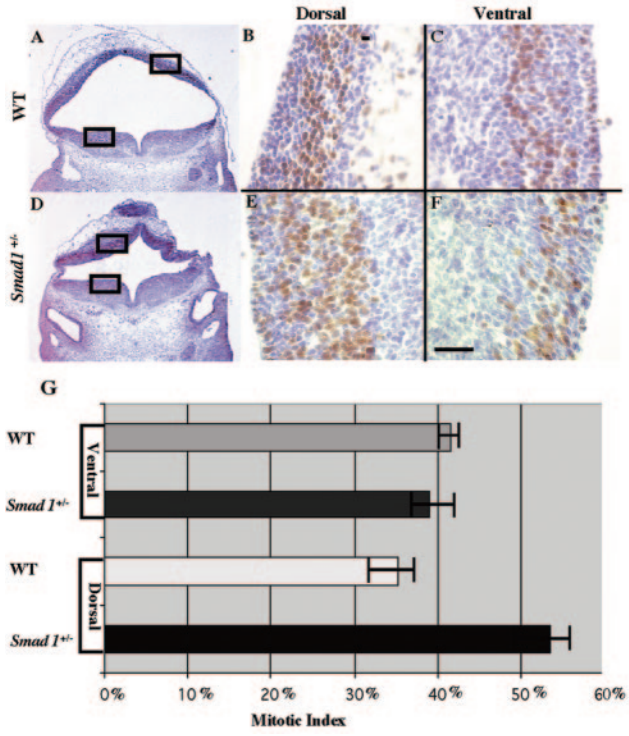

FIG. 6. Phenotypic *Smad1*$^{+/-}$ embryos display increased cellular proliferation in the dorsal region of the neural tube. A histological section stained for BrdU shows a greater number of proliferating cells on the dorsal side of the neural tube in abnormal *Smad1* heterozygotes (D and E) than the wild type (A and B). The boxes in panels A and D indicate the areas enlarged in panels B, C, E, and F. On the ventral side of the neural tube, the number of proliferating cells is equal between *Smad1*$^{+/-}$ (F) and wild-type embryos (C). Quantification of this data shows that there are 20% more proliferating cells on the dorsal side of the neural tube in the *Smad1*$^{+/-}$ embryo than in the wild-type embryo (G).

results were similar in the hindbrain, although cellular proliferation was normal in the spinal cord (data not shown). This indicates that increased cellular proliferation contributes to the observed hypercellularity. Interestingly, this increase appears to be specific to the dorsal region of the midbrain and hindbrain, as no increase in the rate of cellular proliferation was seen in the ventral region of the brain. The level of cellular proliferation was also analyzed in *Smad8*$^{3loxP/3loxP}$ embryos utilizing Ki-67 and phospho-H3 as markers, although we were unable to detect any significant changes between mutant and wild-type embryos. Abnormal *Smad1*$^{+/-}$ and *Smad8*$^{3loxP/3loxP}$ embryos were examined for apoptosis within the neural tube, but no changes were seen (data not shown). We suspect that the *Smad8*$^{3loxP/3loxP}$ embryos do exhibit increased cellular proliferation in the dorsal brain, as evidenced by the observed hypercellularity (Fig. 5E and I). There is more tissue but no increase in cell death. It may be that Ki-67 and phospho-H3 antibodies are insufficient to reveal this increased cellular proliferation, indeed they did not detect proliferative changes in the abnormal *Smad1*$^{+/-}$ embryos.

In an effort to determine the cause of the increased cellular proliferation in the dorsal region of the midbrain and hindbrain, immunohistochemistry was performed to compare the levels of important cell cycle regulatory proteins between wild-type and *Smad1*$^{+/-}$ mutant embryos. This analysis revealed no discernible difference between wild-type and mutant embryos in expression of the cyclin-dependent kinase inhibitor proteins p21 (WAF1/CIP1) and p27 (Kip1) or cyclin D1 (data not shown).

Neurofilament staining of abnormal *Smad1*$^{+/-}$ embryos reveals relatively normal cranial nerve development. The early hindbrain is segmented into discrete units termed rhombomeres from which signals emanate that will orchestrate the development of the nervous system (58). During hindbrain patterning, positional information along the anterior/posterior axis is laid down that allows for the expansion of the peripheral nervous system (54). We therefore wanted to know whether the hindbrain defect observed in abnormal *Smad1* heterozygotes caused a disruption in cranial nerve development. To analyze the anatomy of differentiating neurons in abnormal *Smad1* heterozygotes, we visualized the nervous system at E11.5 by neurofilament staining (12). Careful examination of neurofilament-labeled embryos failed to reveal any drastic changes in cranial nerve development (Fig. 7A and B). Examination of the hindbrain in the phenotypic *Smad1*$^{+/-}$ embryos revealed a curved cranial nerve that is likely to be a secondary effect caused by the abnormal architecture of the hindbrain (Fig. 7B) and not a specific result of *Smad1* disruption. How-

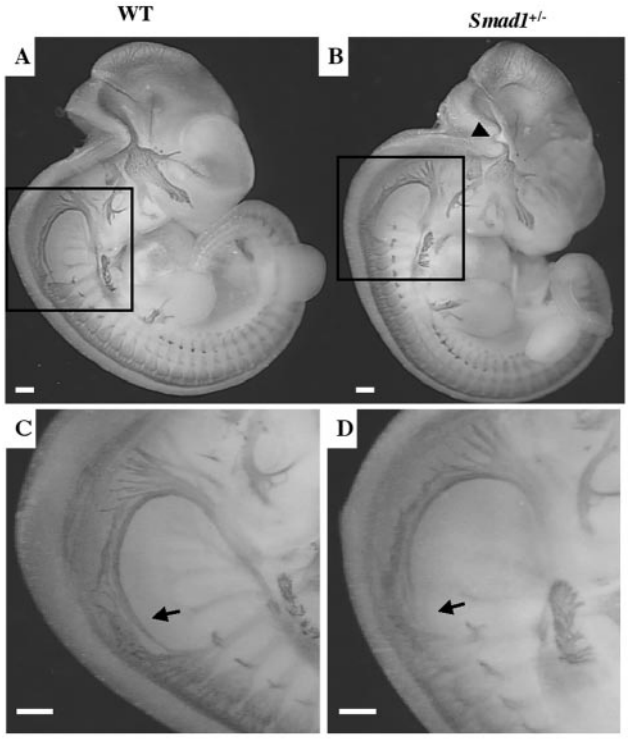

FIG. 7. Abnormal *Smad1*$^{+/-}$ embryos exhibit a truncated spinal accessory nerve. Whole-mount micrograph of a wild-type embryo (A) and a phenotypic *Smad1* heterozygous embryo (B) at E11.5 stained with neurofilament antibody. The *Smad1*$^{+/-}$ hindbrain contains a warped nerve, most likely a secondary effect due to a reduced hindbrain (arrowhead). Higher magnification of the *Smad1*$^{+/-}$ embryo revealed a shortened spinal accessory neuron (XI) (D) compared to the wild type (C).

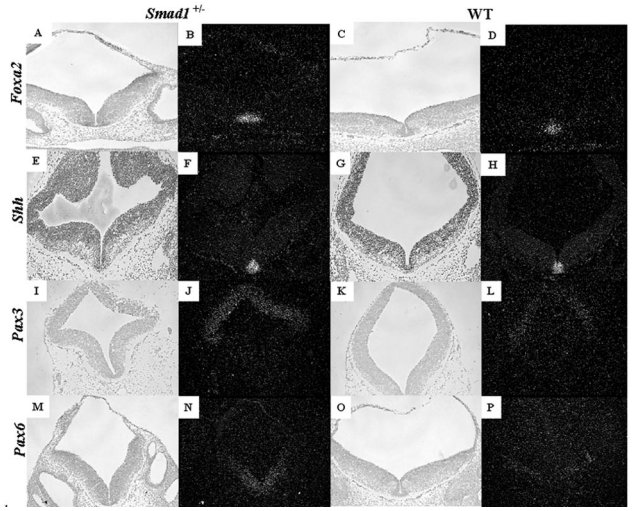

FIG. 8. Examination of genes involved in dorsoventral patterning of the neural tube in phenotypic *Smad1*$^{+/-}$ embryos. Genes that are responsible for ventralizing the neural tube such as *Foxa2* (A to D) and *Shh* (E to H) are expressed at similar levels and similar domains between a phenotypic *Smad1* heterozygous embryo (A and B) and a wild-type embryo (C and D). Bright-field images are shown to the left of the dark-field images. *Pax3* (I to L) and *Pax6* (M to P), genes expressed in the dorsal and ventrolateral regions of the neural tube, respectively, show a significant increase in the *Smad1*$^{+/-}$ embryo (I, J, M, and N) compared to the control embryo (K, L, O, and P).

ever, abnormal *Smad1*$^{+/-}$ embryos exhibited a clearly truncated spinal accessory nerve (Fig. 7C, D), which is more likely to be a direct result of *Smad1* haploinsufficiency.

Examination of genes involved in dorsoventral patterning of the neural tube in phenotypic *Smad1*$^{+/-}$ and *Smad8*$^{3loxP/3loxP}$ embryos. A well-known activity of the BMP family is the patterning of the embryonic neural tube, in which BMPs are expressed dorsally and are thought to promote the formation of dorsal cell fates (16). We therefore undertook an analysis of genes critical in dorsoventral neural tube patterning. *Foxa2* (*Hnf3*β) is expressed in the floor plate and ventral regions of the neural tube in wild-type, *Smad8*$^{3loxP/3loxP}$, and *Smad1*$^{+/-}$ embryos (Fig. 8A to D and 9A to D) and is required for the formation of ventral cell types (2). *Foxa2* was expressed at a similar level and in a similar domain in the wild-type, *Smad1*$^{+/-}$, and *Smad8*$^{3loxP/3loxP}$ phenotypic embryos (Fig. 8A to D and 9A to D), showing that ventral cell fates were not expanded in the *Smad1*$^{+/-}$ and *Smad8*$^{3loxP/3loxP}$ phenotypic embryos. Similar results were seen for *Shh* (Fig. 8E to H and 9E to H), another ventrally expressed gene (17). *Pax3*, a dorsally expressed transcription factor (19, 36), was expressed in its correct domain, although it was upregulated in phenotypic *Smad1* heterozygous and *Smad8*$^{3loxP/3loxP}$ embryos compared to wild-type siblings (Fig. 8I to L and 9I to L). This suggests that the defect seen in the midbrain and hindbrain of the *Smad1*$^{+/-}$ and *Smad8*$^{3loxP/3loxP}$ embryos was not the result of change in the dorsoventral axis within the neural tube. Interestingly, *Pax6* was also upregulated in phenotypic *Smad1* heterozygous and *Smad8*$^{3loxP/3loxP}$ embryos (Fig. 8M to P and 9M to P); however, its expression domain was not expanded and was confined to the intermediate and ventral regions of the neural tube (57).

Changes in spinal cord gene expression in phenotypic *Smad1*$^{+/-}$ embryos. The effects of BMPs in assigning dorsal fate identities within the spinal cord has been studied far more extensively than their dorsalizing capabilities in the brain. One specialized compartment within the dorsal neural tube that requires BMP signals for its propagation and maintenance is the roof plate. This structure is localized at the dorsal midline and formed from glial cells derived from the lateral neural plate (31). Two roof plate markers which have been shown to be responsive to BMP signals, *Id1* and *Msx1* (20, 35), were analyzed in phenotypic *Smad1*$^{+/-}$ embryos for the existence of a roof plate. *Msx1* and *Id1* were both expressed in the roof plate and at similar levels between phenotypic *Smad1*$^{+/-}$ embryos and their wild-type siblings (Fig. 10A to H). These data confirm that the midbrain/hindbrain defect observed in phenotypic *Smad1*$^{+/-}$ embryos is not due to the absence of a roof plate.

Given the increased expression of *Pax3* in the midbrain and hindbrain of the *Smad1*$^{+/-}$ and *Smad8*$^{3loxP/3loxP}$ embryos, we were curious if its expression was normal in the spinal cord. Indeed, *Pax3* was upregulated in the dorsal spinal cord of the *Smad1*$^{+/-}$ (Fig. 9I to L) and *Smad8*$^{3loxP/3loxP}$ mutants (data not shown). Of note, the expression of *Pax3* appears to increased ventrally in the spinal cord (Fig. 9I to L, compare panels J and L), suggesting an increase in dorsal cell fates in the spinal cord. However, an examination of other genes and proteins located along the dorsal/ventral axis in the spinal cord, including *Shh*, *Foxa2*, Ncam, and Isl-1, revealed no differences, nor were there differences in cellular proliferation (data not shown). While examining the anterior/posterior axis of the neural tube in abnormal *Smad1*$^{+/-}$ embryos, the expression of *HoxB9*, a gene

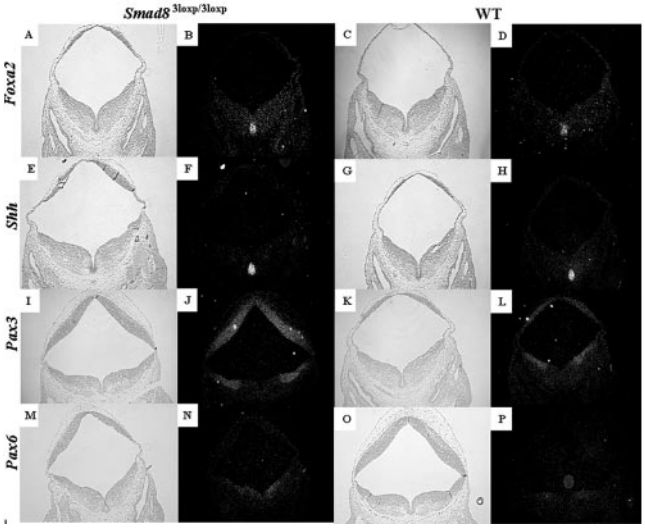

FIG. 9. Examination of genes involved in dorsoventral patterning of the neural tube in phenotypic *Smad8*$^{3loxP/3loxP}$ embryos. Genes that are responsible for ventralizing the neural tube such as *Foxa2* (A to D) and *Shh* (E to H) are expressed at similar levels and similar domains between a phenotypic *Smad8* homozygous embryo (A and B) and a wild-type embryo (C and D). Bright-field images are shown to the left of the dark-field images. *Pax3* (I to L) and *Pax6* (M to P), genes expressed in the dorsal and ventrolateral regions of the neural tube, respectively, show a significant increase in the *Smad8*$^{3loxP/3loxP}$ embryos (I, J, M, and N) compared to the control embryo (K, L, O, and P).

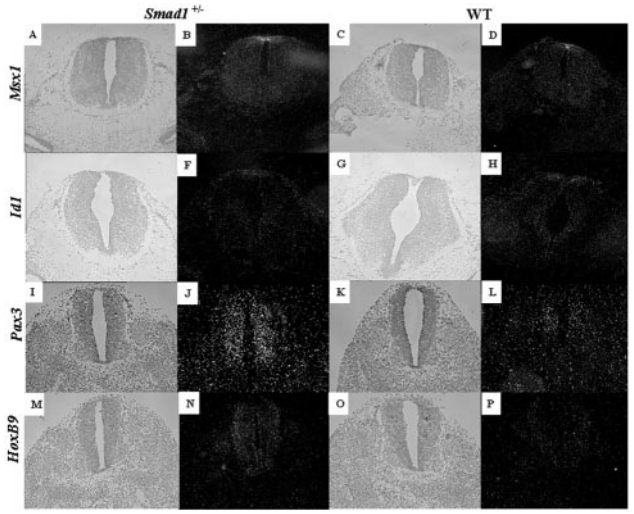

FIG. 10. Analysis of spinal cord markers in phenotypic *Smad1*$^{+/-}$ embryos. BMP-responsive genes that are expressed within the roof plate such as *Id1* (A to D) and *Msx1* (E to H) are expressed at similar levels and similar domains between a phenotypic *Smad1* heterozygous embryo (A, B, E, and F) and a wild-type embryo (C, D, G, and H). Bright-field images are shown to the left of the dark-field images. *Pax3* (I to L) and *HoxB9* (M to P), genes expressed within the spinal cord, show a significant increase in the *Smad1*$^{+/-}$ embryo (I, J, M, and N) compared to the control embryos (K, L, O, and P).

expressed in the spinal cord (51), was examined. Surprisingly, its expression was elevated in abnormal *Smad1* heterozygous embryos compared to their wild-type littermates (Fig. 9M to P). Therefore, although there was no obvious phenotype in the spinal cords of the affected *Smad1*$^{+/-}$ embryos, there were clearly changes in gene expression.

DISCUSSION

Here we have targeted the murine *Smad8* gene, creating two distinct alleles of *Smad8*. One allele, in which exon 3 has been deleted, causes no overt phenotype in the mouse, although it displays reduced ventralizing activity in *Xenopus*. It is probable that some Smad8 functions have become impaired in *Smad8*$^{\Delta exon3/\Delta exon3}$ mice; however, the consequences of this are undetectable under gross examination. Thus, it can be inferred that exon 3 of *Smad8* is dispensable for normal mouse development. The second allele, which contains a *neo* cassette within intron 3, has a 65% reduction of wild-type RNA due to aberrant splicing of *neo* within the *Smad8* transcript. In addition, it creates a truncated product with diminished activity and therefore represents a hypomorphic allele. Intriguingly, we have observed a partially penetrant neuroectodermal defect in 11% of homozygotes of the *Smad8*^{3loxP} allele as well as in 22% of *Smad1* heterozygous embryos.

The *Smad1* and *Smad8* knockouts display an unusual nervous system phenotype. One aspect observed only in phenotypic *Smad1* heterozygous embryos is an increase in cellular proliferation only observed on the dorsal side of the neural tube. This is not due to differences in the expression pattern of Smad1 throughout the neural tube, since it has a ubiquitous expression pattern early in development (10, 55) (M. Hester and M. Weinstein, unpublished data). The increased cellular proliferation is interesting, since application of BMPs to explants of the lateral telencephalon inhibits cell proliferation in vitro (21) and reduction of Smad1 activity would presumably result in decreased BMP signaling.

An increase in *Pax3* expression is also observed in the dorsal mid- and hindbrain of the abnormal *Smad1* and *Smad8* mutants, while *Pax6* expression appears to be elevated ventrally. Using chicken neural explants, it has been shown that increased BMP signaling elevates the level of *Pax3* and *Pax7* as well as the expression of other dorsal neuroectodermal genes (33, 53). From these experiments, it would be expected that phenotypic *Smad8*$^{3loxP/3loxP}$ and *Smad1*$^{+/-}$ embryos would exhibit a decrease in *Pax3* expression. Presumably, the decrease in BMP signaling seen in the affected *Smad1*$^{+/-}$ or *Smad8*$^{3loxP/3loxP}$ embryos is sufficiently subtle that *Pax3* expression might be modulated differently than seen previously. In addition, experiments using chicken neural explants increase the level of BMP signaling to nonphysiological levels.

Another anomaly observed in phenotypic *Smad1* heterozygotes was a shortened spinal accessory nerve (X). Interestingly, it has been shown recently that mutations in the transcription factor *Nkx2.9* cause a shortened spinal accessory nerve (44); otherwise *Nkx2.9*$^{-/-}$ mice are viable and fertile and do not display any behavioral phenotype. Semiquantitative PCR analysis using RNA from phenotypic *Smad1*$^{+/-}$ embryonic brains revealed no significant difference in levels of *Nkx2.9* compared to the wild type (M. Hester and M. Weinstein, unpublished data).

Although BMPs have been shown to dorsalize the embryonic neural tube (25, 31), the phenotypic *Smad1* and *Smad8* embryos did not appear to have abnormal dorsoventral patterning in the brain, in that morphologically distinct floor plates and roof plates were evident in the mutants (Fig. 5E to L). This has been confirmed by normal expression patterns of *Shh*, *Foxa2* (Fig. 8 and 9), *Msx1*, *Id1*, NCAM, and Isl-1 (Hester and Weinstein, unpublished), genes involved in brain development and expressed within narrow dorsoventral boundaries. Although there were increases in the level of *Pax3* and *Pax6* in the abnormal *Smad1* and *Smad8* embryos, the expression domains of these genes did not appear to be changed in the brain (Fig. 8 and 9), further arguing against expansion or reduction of dorsal cell fates within the brain. Interestingly, there appears to be increased expression of *Pax3* ventrally in the spinal cord, suggesting an increase in dorsal cell fates. However, our data suggest that this did not come at the expense of ventral cell fates, nor were any differences seen in the expression of other neuroectodermal genes. This might require further investigation.

Interestingly, another group has constructed a similar *Smad1* knockout allele but has not observed any phenotype associated with *Smad1* heterozygotes (55). A likely explanation for this discrepancy is the presence of modifiers within the different strain backgrounds utilized in these studies (29, 55). The frequency at which *Smad1* heterozygotes (which are on a mixed 129/NIH Black Swiss background) exhibit the observed abnormality can be increased by breeding onto 129Sv/Ev or decreased by breeding onto NIH Black Swiss (Hester and Weinstein, unpublished). Indeed, reductions in the viability of *Smad1* heterozygous mice on a mixed 129Sv/Ev and NIH Black Swiss background were seen in another laboratory (29). This

suggests that there are strain-specific modifiers that affect Smad1 function.

The phenotype seen in the *Smad1*$^{+/-}$ and *Smad8*$^{3loxP/3loxP}$ embryos is not completely penetrant, a phenomenon that has been observed in other knockouts of BMP signaling factors, including *Bmp4* (14) and *Chrd* (1). For example, *Bmp4* homozygous and heterozygous embryos display partially penetrant phenotypes, indicating that the level of Bmp4 is critical for proper development. *Bmp4*$^{-/-}$ embryos die between E6.5 and 9.5, with the majority arresting at the egg cylinder stage due to their inability to gastrulate. The embryos that survive past E6.5 have either unorganized or truncated posterior axes as well as defects in extraembryonic mesoderm formation (59). Interestingly, *Bmp4* heterozygotes also display a range of phenotypes that is dependent upon genetic background. On a mixed 129Sv/Ev and C57BL/6 background, there is no reduction in viability or any significant phenotype associated with *Bmp4* heterozygosity. However, when the *Bmp4* mutation is backcrossed onto the C57BL/6 genetic background, 25% of the heterozygotes die within 3 weeks of birth, exhibiting incompletely penetrant phenotypes such as cystic kidney, polydactyly, microphthalmia, and craniofacial abnormalities (14). Genetic background has also been shown to alter the penetrance of phenotypes observed in *Chrd* knockout mice (1). It is therefore not surprising that the phenotypes we have observed in *Smad1*$^{+/-}$ and *Smad8*$^{3loxP/3loxP}$ embryos are not completely penetrant and that the *Smad1*$^{+/-}$ phenotype is strain dependent.

In summary, we have created hypomorphic alleles for *Smad8*, one of which can function at 35% of the level of wild-type *Smad8*. Interestingly, homozygotes for this allele display a partially penetrant phenotype that phenocopies a hindbrain/midbrain reduction we have observed in *Smad1*$^{+/-}$ embryos at E11.5. Numerous laboratories have shown the importance of BMPs and related family member molecules in nervous system development, but we have for the first time shown the functional importance for their mediators, *Smad1* and *Smad8*, in embryonic brain development. Future studies that delete Smad1 or Smad8 specifically from the embryonic brain utilizing brain-specific Cre strains will be invaluable, allowing the dissection of their functions in brain development.

ACKNOWLEDGMENTS

We thank Natarajan Muthusamy for performing the microinjections of blastocysts to make chimeric *Smad8* mice and Robert Lechleider for generously providing the *Smad1* mutant mice. We also thank Hiroshi Shibuya for kindly providing the Smad8 expression vector and Christoph Plass for obtaining the bacterial artificial chromosome used for generating the Smad8 knockout construct. We are also indebted to Susan Cole and members of the Weinstein laboratory for critical input on this paper.

REFERENCES

1. **Anderson, R. M., A. R. Lawrence, R. W. Stottmann, D. Bachiller, and J. Klingensmith.** 2002. Chordin and noggin promote organizing centers of forebrain development in the mouse. Development **129:**4975–4987.
2. **Ang, S. L., and J. Rossant.** 1994. HNF-3 beta is essential for node and notochord formation in mouse development. Cell **78:**561–574.
3. **Attisano, L., and S. Tuen Lee-Hoeflich.** 2001. The Smads. Genome Biol. **2:**REVIEWS3010.
4. **Attisano, L., and J. L. Wrana.** 2002. Signal transduction by the TGF-beta superfamily. Science **296:**1646–1647.
5. **Bachiller, D., J. Klingensmith, C. Kemp, J. A. Belo, R. M. Anderson, S. R. May, J. A. McMahon, A. P. McMahon, R. M. Harland, J. Rossant, and E. M. De Robertis.** 2000. The organizer factors Chordin and Noggin are required for mouse forebrain development. Nature **403:**658–661.
6. **Chang, H., D. Huylebroeck, K. Verschueren, Q. Guo, M. M. Matzuk, and A. Zwijsen.** 1999. Smad5 knockout mice die at mid-gestation due to multiple embryonic and extraembryonic defects. Development **126:**1631–1642.
7. **Chang, H., A. Zwijsen, H. Vogel, D. Huylebroeck, and M. M. Matzuk.** 2000. Smad5 is essential for left-right asymmetry in mice. Dev. Biol. **219:**71–78.
8. **Deng, C., A. Wynshaw-Boris, F. Zhou, A. Kuo, and P. Leder.** 1996. Fibroblast growth factor receptor 3 is a negative regulator of bone growth. Cell **84:**911–921.
9. **Deng, C. X., A. Wynshaw-Boris, M. M. Shen, C. Daugherty, D. M. Ornitz, and P. Leder.** 1994. Murine FGFR-1 is required for early postimplantation growth and axial organization. Genes Dev. **8:**3045–3057.
10. **Dick, A., W. Risau, and H. Drexler.** 1998. Expression of Smad1 and Smad2 during embryogenesis suggests a role in organ development. Dev. Dyn. **211:**293–305.
11. **Dickinson, M. E., M. A. Selleck, A. P. McMahon, and M. Bronner-Fraser.** 1995. Dorsalization of the neural tube by the non-neural ectoderm. Development **121:**2099–2106.
12. **Dodd, J., S. B. Morton, D. Karagogeos, M. Yamamoto, and T. M. Jessell.** 1988. Spatial regulation of axonal glycoprotein expression on subsets of embryonic spinal neurons. Neuron **1:**105–116.
13. **Ducy, P., and G. Karsenty.** 2000. The family of bone morphogenetic proteins. Kidney Int. **57:**2207–2214.
14. **Dunn, N. R., G. E. Winnier, L. K. Hargett, J. J. Schrick, A. B. Fogo, and B. L. Hogan.** 1997. Haploinsufficient phenotypes in Bmp4 heterozygous null mice and modification by mutations in Gli3 and Alx4. Dev. Biol. **188:**235–247.
15. **Durand, B., P. Sperisen, P. Emery, E. Barras, M. Zufferey, B. Mach, and W. Reith.** 1997. RFXAP, a novel subunit of the RFX DNA binding complex is mutated in MHC class II deficiency. EMBO J. **16:**1045–1055.
16. **Ebendal, T., H. Bengtsson, and S. Soderstrom.** 1998. Bone morphogenetic proteins and their receptors: potential functions in the brain. J. Neurosci. Res. **51:**139–146.
17. **Echelard, Y., D. J. Epstein, B. St-Jacques, L. Shen, J. Mohler, J. A. McMahon, and A. P. McMahon.** 1993. Sonic hedgehog, a member of a family of putative signaling molecules, is implicated in the regulation of CNS polarity. Cell **75:**1417–1430.
18. **el-Hodiri, H. M., and M. Perry.** 1995. Interaction of the CCAAT displacement protein with shared regulatory elements required for transcription of paired histone genes. Mol. Cell. Biol. **15:**3587–3596.
19. **Epstein, J. A.** 2000. Pax3 and vertebrate development. Methods Mol. Biol. **137:**459–470.
20. **Evans, S. M., and T. X. O'Brien.** 1993. Expression of the helix-loop-helix factor Id during mouse embryonic development. Dev. Biol. **159:**485–499.
21. **Furuta, Y., D. W. Piston, and B. L. Hogan.** 1997. Bone morphogenetic proteins (BMPs) as regulators of dorsal forebrain development. Development **124:**2203–2212.
22. **Goulding, M. D., G. Chalepakis, U. Deutsch, J. R. Erselius, and P. Gruss.** 1991. Pax-3, a novel murine DNA binding protein expressed during early neurogenesis. EMBO J. **10:**1135–1147.
23. **Henningfeld, K. A., S. Rastegar, G. Adler, and W. Knochel.** 2000. Smad1 and Smad4 are components of the bone morphogenetic protein-4 (BMP-4)-induced transcription complex of the Xvent-2B promoter. J. Biol. Chem. **275:**21827–21835.
24. **Holzenberger, M., C. Lenzner, P. Leneuve, R. Zaoui, G. Hamard, S. Vaulont, and Y. L. Bouc.** 2000. Cre-mediated germline mosaicism: a method allowing rapid generation of several alleles of a target gene. Nucleic Acids Res. **28:**E92.
25. **Jessell, T. M.** 2000. Neuronal specification in the spinal cord: inductive signals and transcriptional codes. Nat. Rev. Genet. **1:**20–29.
26. **Kao, K. R., and R. P. Elinson.** 1988. The entire mesodermal mantle behaves as Spemann's organizer in dorsoanterior enhanced Xenopus laevis embryos. Dev. Biol. **127:**64–77.
27. **Lai, E., V. R. Prezioso, W. F. Tao, W. S. Chen, and J. E. Darnell, Jr.** 1991. Hepatocyte nuclear factor 3 alpha belongs to a gene family in mammals that is homologous to the Drosophila homeotic gene fork head. Genes Dev. **5:**416–427.
28. **Lakso, M., J. G. Pichel, J. R. Gorman, B. Sauer, Y. Okamoto, E. Lee, F. W. Alt, and H. Westphal.** 1996. Efficient in vivo manipulation of mouse genomic sequences at the zygote stage. Proc. Natl. Acad. Sci. USA **93:**5860–5865.
29. **Lechleider, R. J., J. L. Ryan, L. Garrett, C. Eng, C. Deng, A. Wynshaw-Boris, and A. B. Roberts.** 2001. Targeted mutagenesis of Smad1 reveals an essential role in chorioallantoic fusion. Dev. Biol. **240:**157–167.
30. **Lee, K. J., P. Dietrich, and T. M. Jessell.** 2000. Genetic ablation reveals that the roof plate is essential for dorsal interneuron specification. Nature **403:**734–740.
31. **Lee, K. J., and T. M. Jessell.** 1999. The specification of dorsal cell fates in the vertebrate central nervous system. Annu. Rev. Neurosci. **22:**261–294.
32. **Lee, K. J., M. Mendelsohn, and T. M. Jessell.** 1998. Neuronal patterning by BMPs: a requirement for GDF7 in the generation of a discrete class of commissural interneurons in the mouse spinal cord. Genes Dev. **12:**3394–3407.

33. **Liem, K. F., Jr., G. Tremml, and T. M. Jessell.** 1997. A role for the roof plate and its resident TGFbeta-related proteins in neuronal patterning in the dorsal spinal cord. Cell **91:**127–138.
34. **Liu, Y., M. H. Festing, M. Hester, J. C. Thompson, and M. Weinstein.** 2004. Generation of novel conditional and hypomorphic alleles of the Smad2 gene. Genesis **40:**118.
35. **MacKenzie, A., L. Purdie, D. Davidson, M. Collinson, and R. E. Hill.** 1997. Two enhancer domains control early aspects of the complex expression pattern of Msx1. Mech. Dev. **62:**29–40.
36. **Mansouri, A.** 1998. The role of Pax3 and Pax7 in development and cancer. Crit. Rev. Oncog. **9:**141–149.
37. **Mehler, M. F., P. C. Mabie, D. Zhang, and J. A. Kessler.** 1997. Bone morphogenetic proteins in the nervous system. Trends Neurosci. **20:**309–317.
38. **Meyers, E. N., M. Lewandoski, and G. R. Martin.** 1998. An Fgf8 mutant allelic series generated by Cre- and Flp-mediated recombination. Nat. Genet. **18:**136–141.
39. **Miyanaga, Y., I. Torregroza, and T. Evans.** 2002. A maternal Smad protein regulates early embryonic apoptosis in Xenopus laevis. Mol. Cell. Biol. **22:**1317–1328.
40. **Nagy, A.** 2000. Cre recombinase: the universal reagent for genome tailoring. Genesis **26:**99–109.
41. **Nakayama, T., M. A. Snyder, S. S. Grewal, K. Tsuneizumi, T. Tabata, and J. L. Christian.** 1998. Xenopus Smad8 acts downstream of BMP-4 to modulate its activity during vertebrate embryonic patterning. Development **125:** 857–867.
42. **Nishita, M., N. Ueno, and H. Shibuya.** 1999. Smad8B, a Smad8 splice variant lacking the SSXS site that inhibits Smad8-mediated signalling. Genes Cells **4:**583–591.
43. **Osoegawa, K., M. Tateno, P. Y. Woon, E. Frengen, A. G. Mammoser, J. J. Catanese, Y. Hayashizaki, and P. J. de Jong.** 2000. Bacterial artificial chromosome libraries for mouse sequencing and functional analysis. Genome Res. **10:**116–128.
44. **Pabst, O., J. Rummelies, B. Winter, and H. H. Arnold.** 2003. Targeted disruption of the homeobox gene Nkx2.9 reveals a role in development of the spinal accessory nerve. Development **130:**1193–1202.
45. **Pera, E. M., A. Ikeda, E. Eivers, and E. M. De Robertis.** 2003. Integration of IGF, FGF, and anti-BMP signals via Smad1 phosphorylation in neural induction. Genes Dev. **17:**3023–3028.
46. **Sasai, Y., and E. M. De Robertis.** 1997. Ectodermal patterning in vertebrate embryos. Dev. Biol. **182:**5–20.
47. **Sater, A. K., H. M. El-Hodiri, M. Goswami, T. B. Alexander, O. Al-Sheikh, L. D. Etkin, and J. Akif Uzman.** 2003. Evidence for antagonism of BMP-4 signals by MAP kinase during Xenopus axis determination and neural specification. Differentiation **71:**434–444.
48. **Sauer, B., and N. Henderson.** 1988. Site-specific DNA recombination in mammalian cells by the Cre recombinase of bacteriophage P1. Proc. Natl. Acad. Sci. USA **85:**5166–5170.
49. **Solloway, M. J., and E. J. Robertson.** 1999. Early embryonic lethality in Bmp5;Bmp7 double mutant mice suggests functional redundancy within the 60A subgroup. Development **126:**1753–1768.
50. **Suzuki, A., C. Chang, J. M. Yingling, X. F. Wang, and A. Hemmati-Brivanlou.** 1997. Smad5 induces ventral fates in Xenopus embryo. Dev. Biol. **184:** 402–405.
51. **Suzuki, M., Y. Mizutani-Koseki, Y. Fujimura, H. Miyagishima, T. Kaneko, Y. Takada, T. Akasaka, H. Tanzawa, Y. Takihara, M. Nakano, H. Masumoto, M. Vidal, K. Isono, and H. Koseki.** 2002. Involvement of the Polycomb-group gene Ring1B in the specification of the anterior-posterior axis in mice. Development **129:**4171–4183.
52. **Thomsen, G. H.** 1996. Xenopus mothers against decapentaplegic is an embryonic ventralizing agent that acts downstream of the BMP-2/4 receptor. Development **122:**2359–2366.
53. **Timmer, J. R., C. Wang, and L. Niswander.** 2002. BMP signaling patterns the dorsal and intermediate neural tube via regulation of homeobox and helix-loop-helix transcription factors. Development **129:**2459–2472.
54. **Trainor, P. A., and R. Krumlauf.** 2000. Patterning the cranial neural crest: hindbrain segmentation and Hox gene plasticity. Nat. Rev. Neurosci. **1:**116–124.
55. **Tremblay, K. D., N. R. Dunn, and E. J. Robertson.** 2001. Mouse embryos lacking Smad1 signals display defects in extra-embryonic tissues and germ cell formation. Development **128:**3609–3621.
56. **Walther, C., and P. Gruss.** 1991. Pax-6, a murine paired box gene, is expressed in the developing CNS. Development **113:**1435–1449.
57. **Warren, N., and D. J. Price.** 1997. Roles of Pax-6 in murine diencephalic development. Development **124:**1573–1582.
58. **Wilkinson, D. G., and R. Krumlauf.** 1990. Molecular approaches to the segmentation of the hindbrain. Trends Neurosci. **13:**335–339.
59. **Winnier, G., M. Blessing, P. A. Labosky, and B. L. Hogan.** 1995. Bone morphogenetic protein-4 is required for mesoderm formation and patterning in the mouse. Genes Dev. **9:**2105–2116.
60. **Wozney, J. M., V. Rosen, A. J. Celeste, L. M. Mitsock, M. J. Whitters, R. W. Kriz, R. M. Hewick, and E. A. Wang.** 1988. Novel regulators of bone formation: molecular clones and activities. Science **242:**1528–1534.
61. **Wrana, J. L.** 2000. Crossing Smads. Sci. STKE **2000:**RE1.
62. **Wrana, J. L., and L. Attisano.** 2000. The Smad pathway. Cytokine Growth Factor Rev. **11:**5–13.
63. **Xu, X., C. Li, L. Garrett-Beal, D. Larson, A. Wynshaw-Boris, and C. X. Deng.** 2001. Direct removal in the mouse of a floxed neo gene from a three-loxP conditional knockout allele by two novel approaches. Genesis **30:**1–6.
64. **Yang, X., L. H. Castilla, X. Xu, C. Li, J. Gotay, M. Weinstein, P. P. Liu, and C. X. Deng.** 1999. Angiogenesis defects and mesenchymal apoptosis in mice lacking SMAD5. Development **126:**1571–1580.
65. **Zhao, G. Q.** 2003. Consequences of knocking out BMP signaling in the mouse. Genesis **35:**43–56.